

¹ **Highlights**

² **A Wearable Thumb Device for Fruit Firmness Estimation with Vision-Based Tactile Sensing**

³ Mashhood M. Mohsan, Basma B. Hasanen, Taimur Hassan, Lakmal Seneviratne, Irfan Hussain

⁴ • A novel wearable device for non-destructive, and real-time fruit firmness estimation is proposed.

⁵ • A deep learning model is proposed and deployed on the device with a R^2 of 0.89%.

⁶ • A "Hayward" Kiwi dataset with 530 pairs of tactile palpation and penetrometer firmness readings
⁷ was collected to validate the device.

⁸ • The device was validated for real-time firmness, demonstrating its practicality in agriculture.

9 A Wearable Thumb Device for Fruit Firmness Estimation with Vision-Based
10 Tactile Sensing

11 Mashhood M. Mohsan^{a,b,1}, Basma B. Hasanen^{a,b,1}, Taimur Hassan^c, Lakmal Seneviratne^{a,b}, Irfan
12 Hussain^{a,b,*}

13 ^a*Khalifa University Center for Autonomous Robotic Systems (KUCARS), Khalifa University, UAE.*

14 ^b*Department of Mechanical and Nuclear Engineering, Khalifa University, Abu Dhabi, 127788, United Arab Emirates*

15 ^c*Department of Electrical, Computer and Biomedical Engineering, Abu Dhabi University, UAE.*

16 **Abstract**

Recent advancements in non-destructive technologies have enabled precise firmness measurement for various fruits, including kiwifruit. However, existing methods remain limited by high costs, environmental sensitivity, and field application impracticality. This work introduces a novel wearable device for estimating non-destructive fruit firmness, combining human tactile interaction with vision-based tactile sensing and edge computing. Worn on the thumb, the device leverages embodied intelligence, merging intuitive human touch with the precision of a vision-based tactile sensor. A single-board computer processes tactile images locally, enabling reliable operation even in remote environments. The device employs our proposed deep learning model for real-time firmness predictions from a single palpation, minimizing repetitive handling and reducing fruit bruising. Its ergonomic, symmetrical design supports comfortable use on either hand, enhancing usability. Compact and portable, the device integrates essential components within a housing measuring 40 mm × 25 mm × 72 mm and weighing only 135 g. Validated through non-destructive ripeness assessments on 'Hayward' Kiwifruit, the device demonstrated a strong correlation between tactile images and firmness values when paired with our proposed model, achieving a coefficient of determination (R^2) of 0.89. This study created a dedicated dataset on Kiwi firmness to support model development and validation. Moreover, this work's proposed dataset and source code will be released publicly upon paper acceptance.

17 **Keywords:** Vision-Based Tactile Sensing, Deep Learning, Wearable, Agricultural device, Firmness

18 **1. Introduction**

19 Each year, approximately one billion tons of food are wasted globally, intensifying food insecurity
20 and underscoring the urgent need for sustainable practices in the food industry (Voss et al. 2024). Fruit
21 production is particularly critical, as rising consumer demand for high-quality produce increases pressure
22 to minimize losses. Efficient quality assessment plays a key role in addressing this challenge.

23 Ripeness is a fundamental measure of fruit quality, directly influencing taste, and marketability. Accurate
24 ripeness evaluation ensures fruits are harvested at their optimal maturity, enhancing flavor, nutritional

*Corresponding Author

Email addresses: mashood.mohsan@ku.ac.ae (Mashhood M. Mohsan), basma.hasanen@ku.ac.ae (Basma B. Hasanen), taimur.hassan@adu.ac.ae (Taimur Hassan), lakmal.seneviratne@ku.ac.ae (Lakmal Seneviratne), irfan.hussain@ku.ac.ae (Irfan Hussain)

¹Authors equally contributed to this work.

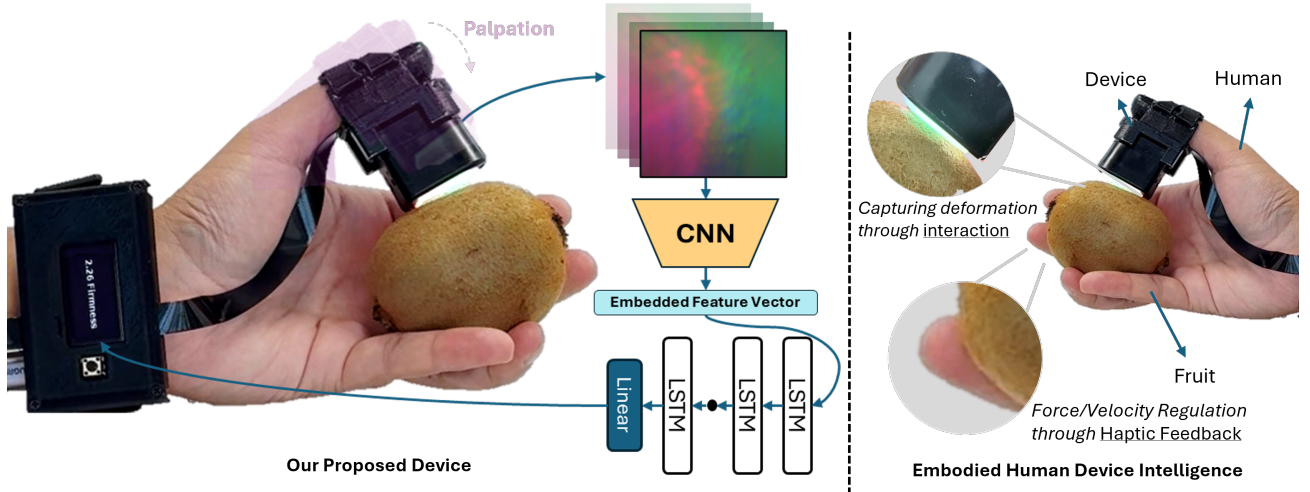


Figure 1: The proposed wearable device for real-time, and non-destructive fruit firmness estimation. The user palpates a Kiwi, and the proposed model processes the VBTS palpation recording to predict firmness in a non-destructive approach. The right segment illustrates the concept of embodied human-device intelligence, highlighting how haptic feedback and human interaction regulate force during palpation.

value, and storage potential. It also reduces waste during distribution and increases consumer satisfaction, providing a competitive edge for producers (Mazhar et al. 2016)(Khalifa, Mohammad Hassan Komarizadeh, and Tousi 2011).

For fruits such as mangoes, bananas, and apples, ripeness is often determined by visible skin color changes, with computer vision (CV)-based solutions providing non-invasive and effective assessments (Valliente, Parco, and Sangalang 2021). In contrast, fruits such as Kiwis, which show little to no color change during ripening, rely on firmness as a more reliable indicator of maturity and readiness for consumption. This is especially crucial for Kiwifruit, valued for its high nutritional content and economic significance. An accurate assessment of firmness is essential to maintain quality, preserve market appeal, and minimize waste (Nazir et al. 2024; Khan et al. 2023). Moreover, Kiwifruit's susceptibility to bruising during handling highlights the importance of gentle and precise evaluation methods to ensure quality. (Ahmadi 2018; F. R. Harker and Hallett 1994).

Although various non-destructive tools have been explored, many are constrained by operator dependence, environmental sensitivity, and limited adaptability across different fruit types (J. Abbott et al. 1995; Anjali et al. 2024). Vision-based tactile sensing (VBTS) has recently emerged as a promising alternative, capturing high-resolution deformation data through soft elastomeric interfaces. When coupled with deep learning, these systems offer improved accuracy and robustness for firmness estimation under variable conditions (Ma, Ying, and Xie 2024; J. Lin et al. 2023; Yuan, Srinivasan, and Adelson 2016; Yuan, Zhu, et al. 2017; Mohsan et al. 2025). Building on the strengths of VBTS while addressing the limitations of existing tools, we present a novel wearable device specifically designed for fruits like kiwifruit, where firmness is a key ripeness indicator. The device, worn on the thumb, naturally follows the motion of human touch to apply controlled, gentle pressure to the fruit's surface (Figure 1). An integrated RGB camera records deformation in the elastomer, and deep learning algorithms process these patterns to predict firmness with high precision. To the best of our knowledge, this is the first system to integrate VBTS principles with human tactile dynamics in a wearable form, enabling non-destructive, intuitive, and accurate firmness assessment.

A key advantage of the device is its efficiency, as it determines Kiwifruit ripeness in a single palpation

51 motion—unlike humans, who often require multiple attempts, increasing the risk of bruising (Rivera et al.
52 2023; Barrett, E. Garcia, and and 1998). The design leverages natural haptic feedback from the supporting
53 fingers, enabling real-time pressure adjustments. In comparison to robotic systems, which often prioritize
54 precision but lack adaptability (Mohsan et al. 2025), the wearable device integrates advanced sensors with
55 the human ability to intuitively adjust force. This hybrid approach ensures accurate, efficient, and gentle
56 handling of delicate fruits like Kiwifruit. By merging automation with human intuition, the device provides
57 a sustainable and reliable solution for enhancing firmness evaluation while minimizing damage, ultimately
58 improving fruit quality.

59 This paper has the following key contributions:

- 60 1. A novel wearable thumb device for non-destructive fruit firmness estimation, integrating a vision-
61 based tactile sensor (VBTS) to capture localized surface deformations during palpation. This AI-
62 driven approach, which combines human intelligence with VBTS analysis, is, to the best of our
63 knowledge, the first of its kind.
- 64 2. A deep learning model is proposed and deployed on a compact single-board computer, enabling local
65 video-based inference to estimate firmness by extracting spatial and temporal features from tactile
66 palpation.
- 67 3. A "Hayward" Kiwifruit dataset was collected, comprising tactile palpation recordings and penetrometer-
68 based firmness measurements to develop and validate the proposed device. This dataset and the source
69 code of the proposed model will be publicly available upon acceptance.
- 70 4. The proposed wearable device was validated for firmness assessment through field experiments,
71 demonstrating its practicality for non-destructive, real-time firmness evaluation in agriculture.

72 **2. Related Work**

73 *2.1. Traditional Methods of Fruit Firmness Estimation*

74 Mechanical devices for evaluating fruit firmness typically utilize compression, puncture, and impact
75 tests (H. Li et al. 2016). Among invasive methods, the Magness-Taylor (MT) penetrometer remains a widely
76 adopted tool for measuring rupture force by inserting a probe into the fruit (Judith A Abbott 1999). However,
77 the reliance on operator skill in using these devices introduces variability in results (F. Harker, Maindonald,
78 and Jackson 1996). To address this challenge, advancements such as force gauges mounted on controlled
79 stands have been developed to enhance precision (Jantra et al. 2018). Despite these improvements, the
80 inherently invasive nature of these devices poses a significant limitation, as the tested samples are unusable
81 afterwards.

82 In contrast, non-invasive mechanical devices, like durometers, assess parameters such as resistance or
83 biyyield force with minimal damage to the fruit. However, their accuracy depends on user technique, and
84 they often require reconfiguration for different fruit varieties, reducing their versatility (F. Harker, Maindon-
85 ald, and Jackson 1996). Beyond mechanical approaches, acoustic and vibrational methods have emerged as
86 promising non-invasive alternatives for assessing firmness. Acoustic devices operate by generating sound
87 waves through impact excitation and analyzing the resulting signals to determine fruit firmness (Khalifa,
88 Mohammad Hasan Komarizadeh, and Tousi 2011). Vibrational methods, on the other hand, involve generat-
89 ing vibrations and detecting the response, which is influenced by the resonance frequency of the fruit and
90 correlates closely with its firmness. While promising, these methods remain susceptible to environmental

91 factors such as temperature, humidity, and background noise, affecting their reliability in field conditions
92 (J. Abbott et al. 1995).

93 Additionally, optical methods provide advanced non-invasive techniques for firmness evaluation, utilizing
94 visible and near-infrared (NIR) spectra to measure various quality attributes. Reflectance-based optical
95 devices capture diffusing reflectance spectra to construct predictive models for firmness-related parameters,
96 as demonstrated by handheld NIR analyzers and portable Vis/NIR spectrometers (Cirilli et al. 2016; Huang,
97 Lu, and K. Chen 2018). Transmittance-based optical devices complement these approaches by measuring
98 light that passes through the fruit, offering valuable insights into internal quality attributes. However, these
99 systems can be costly and sensitive to variations in fruit surface properties such as color, texture, and shape.
100 Additionally, environmental factors like dust, moisture, and surface damage can introduce inconsistencies,
101 necessitating careful calibration (Anjali et al. 2024).

102 *2.1.1. Wearable Devices for Fruit Firmness Estimation*

103 Advancements in wearable technology have revolutionized non-destructive testing methods, enhancing
104 the efficiency and precision of fruit firmness estimation during harvesting and quality assessment. K. Peleg
105 et al. pioneered a method utilizing vibration and acceleration transducers to evaluate the firmness of fruits
106 and vegetables without causing damage (Peleg 1997). Expanding on this foundation, Q. Lin et al. developed
107 a wearable glove device capable of detecting and classifying agricultural products by measuring their
108 curvature, color, and weight (C.-D. Lin et al. 2018). Similarly, C. Pinto et al. introduced an intelligent glove
109 equipped with sensors for pressure, color, and flexion, enabling real-time analysis of produce maturity and
110 quality (Pinto et al. 2014).

111 Current wearable firmness estimation devices rely on low-resolution sensors, restricting their capability
112 to capture detailed palpation and texture variations. Research on vision-based tactile sensing in wearable
113 devices, which provides higher resolution and enhanced sensitivity, remains unexplored, despite its potential
114 for more precise firmness assessment.

115 *2.1.2. Visuo-Tactile-based Devices for Fruit Firmness Estimation*

116 Visuo-tactile devices have emerged as innovative tools for evaluating fruit firmness, a crucial factor in
117 agricultural quality control. These devices facilitate non-destructive firmness measurements by seamlessly
118 integrating advanced visual and tactile sensing technologies, significantly enhancing harvesting and storage
119 practices. For instance, a visuo-tactile sensor designed to detect image variations during touch demonstrated
120 remarkable efficacy, achieving an R^2 of 0.88 and an RMSE of 0.719 in assessing peach firmness (Ma, Ying,
121 and Xie 2024). Similarly, a device employing a soft gripper inspired by the fin-ray effect combined tactile
122 sensing with visual data processing, achieving R^2 values of 0.795 for tomatoes and 0.753 for nectarines
123 (J. Lin et al. 2023). Another approach utilizes tactile predictive recognition for evaluating fruit hardness,
124 delivering superior accuracy compared to conventional methods (S. Li et al. 2023).

125 Existing non-destructive fruit firmness estimation devices face several limitations. Mechanical devices
126 like durometers depend on operator skill and are often fruit-specific, requiring additional assembly for different varieties (F. Harker, Maindonald, and Jackson 1996). Acoustic and vibrational methods are affected
127 by environmental factors such as temperature, humidity, and noise, compromising accuracy (J. Abbott et
128 al. 1995). Optical devices, while advanced, are costly and inconsistent due to variations in fruit surface
129 properties and environmental conditions like dust, moisture, and surface damage (Anjali et al. 2024). To
130 overcome these challenges, we propose a novel wearable device that utilizes a vision-based tactile sensor for
131 estimating fruit firmness. This device, designed for quality inspectors and farmers, is the first nondestructive
132 approach to leverage off-the-shelf VBTS for mimicking human palpation. Worn on the thumb, it applies
133 human-level pressure to the fruit surface, causing deformation in an elastomer. The RGB camera captures

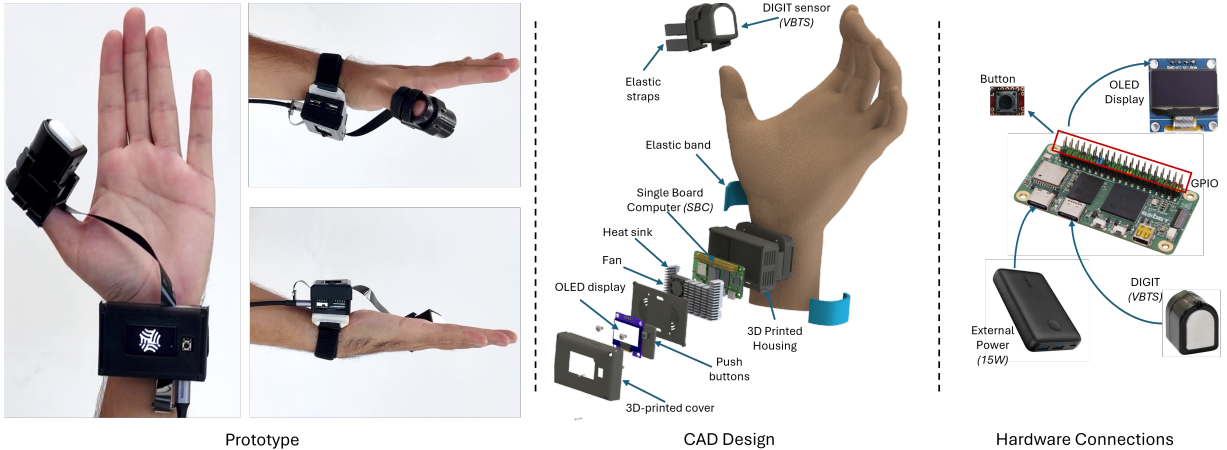


Figure 2: **Development of proposed device** (Left) The prototype of proposed device. (Center) A CAD exploded view of our device, illustrating its two main modules: the thumb module with a VBTS at the tip of the thumb and the wrist module containing the main control unit and user interaction interface in the 3D-printed housing. Adjustable elastic straps are used in both modules for secure and comfortable use. (Right) Hardware setup and connections: The Radxa Zero 2 Pro is connected with one button, an OLED display, a DIGIT (VBTS) sensor, and an external power bank of 15W is used.

135 this deformation, and a deep learning model processes the data to predict firmness, enabling accurate and
136 efficient ripeness grading.

137 3. Materials and Methods

138 The proposed wearable device, illustrated in Figure 1, was designed for the non-destructive, and real-
139 time firmness assessment of 'Hayward' kiwifruit. This section describes the device's working principle
140 and design, including integrating embedded systems for real-time processing. It also describes the plant
141 material used, highlighting the creation of a dedicated dataset comprising tactile palpation recordings paired
142 with penetrometer-based firmness measurements for model development. Furthermore, it also describes the
143 proposed model and the implementation details that enabled accurate firmness estimation.

144 3.1. Embodied Human-Device Intelligence

145 Embodied intelligence (Zhao et al. 2024), in the context of this paper, represents the seamless integra-
146 tion of human tactile abilities with advanced technological tools to achieve reliable and accurate firmness
147 assessments. Haptic feedback, combining tactile and proprioceptive sensors, is fundamental to human
148 touch. Tactile receptors detect changes in pressure, deformation, and contact area, while proprioceptive
149 sensors in muscles and joints monitor finger movement and position. Together, these sensory inputs create a
150 feedback loop that allows humans to adapt force precisely to material compliance without causing damage
151 (Xu et al. 2020; Condon et al. 2014).

152 Despite this sophistication, human tactile assessments are inherently variable and often inconsistent.
153 Repeated palpation, commonly used to verify firmness, can be destructive, particularly for delicate objects
154 like fruits. Furthermore, humans may forget or misinterpret past tactile experiences, leading to unreliable
155 evaluations. To overcome these challenges, our wearable device augments human capabilities, combining
156 the adaptability of human touch with the precision and consistency of the device. The processing unit
157 processes tactile information captured by the vision-based tactile sensor with reliability, ensuring accurate
158 firmness assessments.

159 This synergy between human and device embodies intelligence by leveraging the operator's tactile in-
160 stincts while standardizing and enhancing the assessment process. The device captures and processes tactile
161 information in real time, providing an objective assessment with a single palpation, unlike humans, who of-
162 ten rely on repeated comparisons to discern relative firmness.

163 *3.2. Device Design*

164 The proposed device comprises two primary modules: a thumb module and a wrist module. The thumb
165 module, worn on the user's thumb, incorporates a vision-based tactile sensor (DIGIT) at its tip (Lambeta
166 et al. 2020), enabling high-resolution sensing of contact deformations during human palpation. The DIGIT
167 sensor captures rich, real-time tactile data by observing the deformation of a soft elastomer surface through
168 an internal camera, allowing for accurate recording of subtle textures, pressures, and natural interactions
169 with the fruit. The wrist module contains the main control unit, a display, and a single user-friendly button
170 for straightforward interaction. The device was designed symmetrically to accommodate different user
171 preferences, allowing comfortable use on either hand. Figure 2 illustrates the Computer-Aided Design
172 (CAD) of our device.

173 To validate its design and functionality, a prototype was developed (Figure 2). Both the wrist and thumb
174 holders were 3D printed using black polylactic acid (PLA) filament. For additional comfort, the base of
175 the wrist module was manufactured with a flexible NinjaFlex thermoplastic polyurethane (TPU). This was
176 done to ensure a comfort fit on user's wrist. An adjustable soft strap was then attached to the base of wrist
177 module and thumb module allowing the device to fit users of different sizes, making the thumb wearable
178 both adaptable and secure during operation.

179 *3.3. Embedded System*

180 Local data processing is essential for our device to operate in remote locations where network con-
181 nectivity is unreliable. To achieve this, the device was designed as a complete stand-alone unit for on-site
182 inference. This approach ensures continuous operation and low latency.

183 At the core of the proposed system is the Radxa Zero 2 Pro single-board computer (SBC). This SBC
184 is equipped with a quad-core ARM Cortex-A53 processor, a Mali-G31 MP2 GPU, up to 4GB of LPDDR4
185 RAM, and eMMC storage, providing edge computational power for real-time tactile data processing. For
186 user interaction, an OLED display was integrated into the system to provide visual feedback, and a button
187 was included to initiate operations. The DIGIT VBTS (Lambeta et al. 2020), attached on the thumb module,
188 captures high-resolution tactile palpation information, which are then processed locally on the SBC. Power
189 is supplied through an external power source. All peripherals, including the display, buttons, VBTS, and
190 power bank, are connected to the SBC via its General-Purpose Input/Output (GPIO) interface, establishing
191 a centralized control system. Figure 2 illustrates the hardware connections.

192 The operation workflow begins when the user presses the button, triggering the palpation process. The
193 DIGIT sensor captures tactile images in the form of video, which are then processed by our proposed deep
194 learning model deployed on the SBC. The model analyzes the palpation video in real time to predict the
195 firmness of the object under examination. The firmness value is displayed on the OLED screen.

196 *3.4. Plants Materials*

197 This section describes how the dataset was gathered, including selection of fruit, acquisition protocols,
198 and labeling methods, all crucial for training and validating the model.

199 The Hayward Kiwifruit variety was selected for this study due to its widespread cultivation and its
200 reputation for superior quality and appealing flavor (C. V. Garcia et al. 2012). This variety is known for

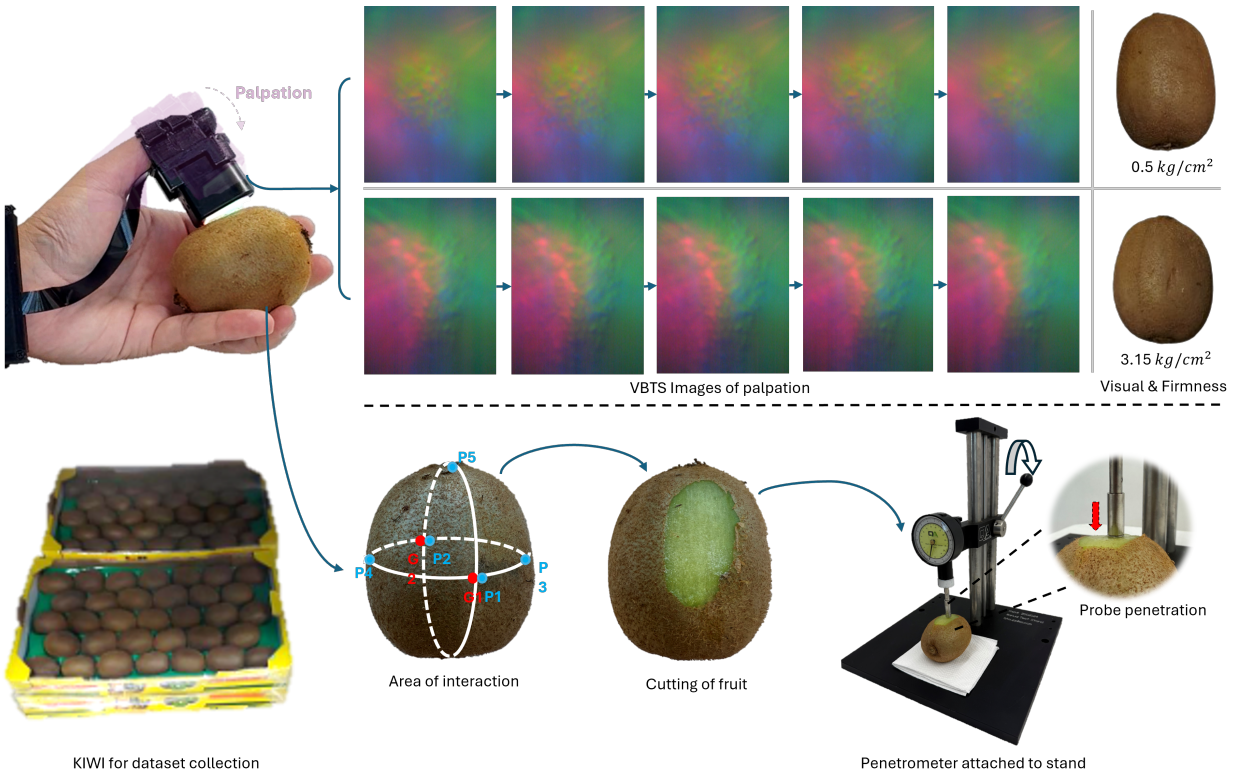


Figure 3: Illustration of the dataset collection: The proposed device is used to record palpation data from each fruit. On the top right, two representative samples are shown—one soft ($0.5 \text{ kg}/\text{cm}^2$) and one firm ($3.15 \text{ kg}/\text{cm}^2$). Although both appear visually similar, their VBTS palpation signatures differ significantly, reflecting variations in firmness. At the bottom center, the blue points mark where each sample is palpated, and the red point indicates where the penetrometer reading is taken. Each Kiwi is then cut for penetrometer based ground truth measurements (Bottom right).

201 its gradual decline in firmness during ripening, driven by physiological changes. Initially firm at harvest,
202 the fruit softens over time as cell adhesion weakens during cold storage. This softening accelerates in the
203 later stages of ripening due to increased cell separation and greater plasticity of cell walls. These changes
204 make accurate firmness assessment essential for maintaining fruit quality during post-harvest handling and
205 storage (F. R. Harker and Hallett 1994).

206 A total of 106 fruit samples were randomly selected for this study. Each fruit was palpated using the
207 device at five distinct points (P1–P5) to capture localized variations in firmness. Ground truth firmness
208 was measured using a QA Supplies penetrometer (Supplies n.d.). According to the standard protocol,
209 approximately 1 mm of the fruit peel was removed to expose a flat flesh surface, and the probe was inserted
210 perpendicularly into the fruit flesh to a depth of 7.9 mm (5/16 inch) over the course of a few seconds
211 (Magness and Taylor 1925; H. Li et al. 2016). Readings were considered invalid if the probe was inserted
212 beyond or fell short of this marked depth. The penetrometer measured firmness in units of kg/cm^2 .

213 Firmness values (G1 and G2) for each fruit were measured at only two equatorial points, either P1–P2 or
214 P3–P4, and the average of the two values was used as the ground truth. The P5 point, located near the stem,
215 was not used for penetration-based firmness measurement, as creating a flat surface in this curved region
216 would require the removal of fruit flesh, thereby violating the standard protocol. However, we intentionally
217 included P5 in our sampling protocol for recording palpation only to ensure the dataset reflects real-world
218 variability and improves the generalizability of our device across different fruit regions. Figure 3 illustrates
219 the dataset collection process and how the VBTS signatures differ between soft and hard samples.

220 This procedure yielded 530 unique pairs of VBTS palpation recordings and corresponding ground truth
221 measurements. For each palpation recording, frames were selected from the start of contact until the end
222 of contact. The number of frames per recording ranged from 32 to 96, with a mean of 44.32 (median 43).
223 Ground truth firmness values ranged from 0.5 to 3.3 kg/cm^2 , with a mean of 1.4945 kg/cm^2 (median 1.45
224 kg/cm^2). While most samples clustered around the mean, a few outliers extended the range, especially very
225 hard fruits. Finally, the dataset was split in an 80:20 ratio for training and testing, ensuring that the model
226 is evaluated across the complete firmness spectrum—including atypical values.

227 3.5. Network Architecture and Implementation Details

228 This study proposes a CNN-LSTM architecture for predicting fruit firmness from video sequences (Figure 4). The model input consists of 16-frame sequences uniformly sampled from each video, ensuring
229 consistent temporal coverage. Spatial features are extracted from individual frames using a pre-trained
230 MobileNet v2 (Howard et al. 2017), which processes the spatial information within each frame. These ex-
231 tracted features are then passed to a single-layer LSTM with 128 hidden units, enabling the model to capture
232 temporal dependencies across the sampled frames. This approach allows the CNN-LSTM architecture to
233 effectively analyze palpation videos and estimate fruit firmness with high precision.

234 To ensure uniform temporal representation of the video data, frames were sampled at equal intervals.
235 The sampling process divided the total number of frames, N , into consistent intervals corresponding to the
236 desired number of sampled frames, n_{sample} . The step size is determined using the formula:

$$\text{step} = \max\left(1, \frac{N - 1}{n_{sample} - 1}\right)$$

237 The Huberloss (Huber 1992) loss function optimizes the model’s performance during training. It is
238 defined as:

$$L(y, \hat{y}) = \begin{cases} 0.5 \cdot (y - \hat{y})^2 & \text{if } |y - \hat{y}| \leq \delta, \\ \delta \cdot |y - \hat{y}| - 0.5 \cdot \delta^2 & \text{otherwise.} \end{cases}$$

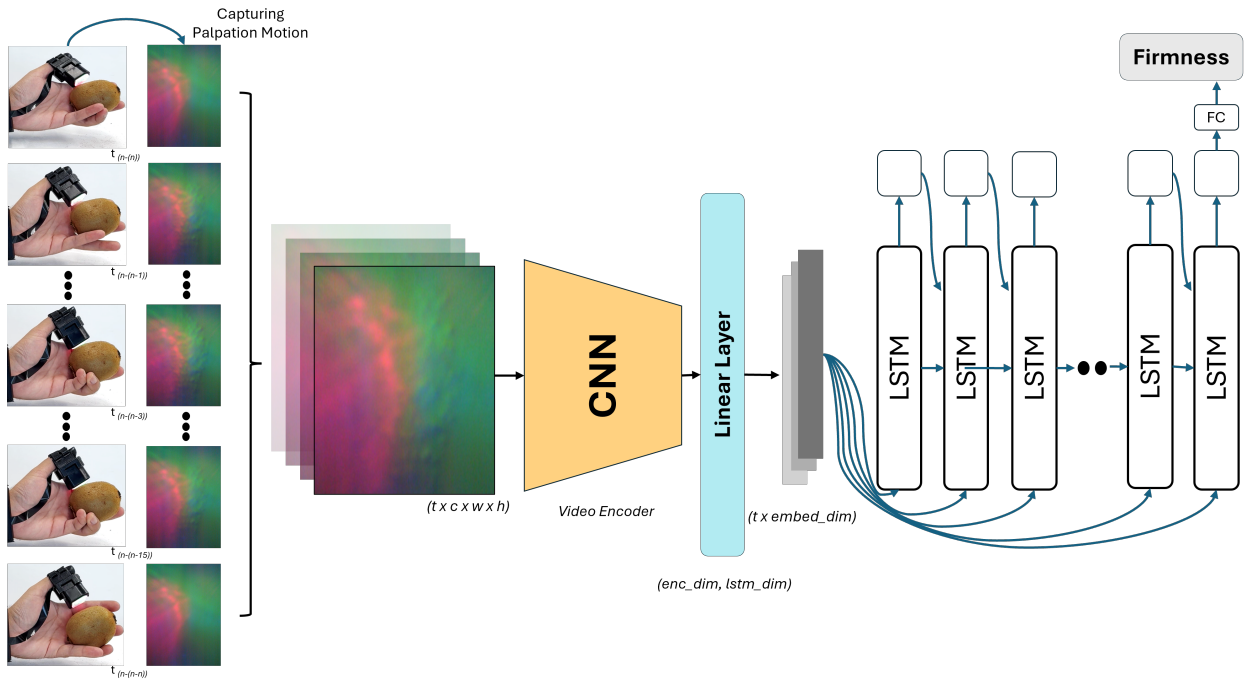


Figure 4: **Proposed architecture:** VBTS palpation recordings, captured over n frames, are processed by a CNN-based video encoder to extract spatial features. A linear layer transforms these features at each time step into 1D spatial representations, subsequently fed into an LSTM network to model temporal dependencies. The final output is passed through a fully connected (FC) layer, generating the firmness prediction of the Kiwi.

240 Here, y represents ground truth, \hat{y} represents predicted firmness, and δ represents the threshold at which the
241 loss transitions from quadratic to linear, enhancing its robustness to outliers.

242 The training process employed the RMSprop optimizer and a CosineAnnealingLR scheduler to optimize
243 the network's performance. Early stopping was applied after five epochs of no improvement to prevent
244 overfitting. Pre-trained weights were fine-tuned over 1000 epochs with a learning rate and weight decay
245 of 0.00005. Data augmentation techniques were employed to improve generalization, including random
246 horizontal flipping, color jittering, and normalization.

247 The proposed model was implemented with Pytorch using the HuggingFace library on a machine with
248 NVIDIA RTX 4090 GPU, CUDA Toolkit v11.0.221, and cuDNN v7.5. The effectiveness of the proposed
249 model in estimating firmness is comprehensively assessed and benchmarked against state-of-the-art (SOTA)
250 methods using evaluation metrics such as Mean Absolute Error (MAE), Mean Squared Error (MSE), Root
251 Mean Squared Error (RMSE), and Coefficient of Determination (R^2).

252 4. Experimentation on CNN-LSTM model

Table 1: Experimenting with the proposed model's various components and parameters as discussed in Section 4. In Exp# 1, the *Sample Duration* was experimented with for better temporal context. Exp# 2 explores the impact of *Loss Functions* for better accuracy, and lastly, in Exp# 3, the effect of optimizer was explored for convergence.

Sr	Model	Sample Duration	Loss function	Optimizer	$R^2 \uparrow$
1	Baseline	8	SmoothL1	AdamW	0.70
2	Exp# 1	4	SmoothL1	AdamW	0.43
3		16	SmoothL1	AdamW	0.79
4	Exp# 2	16	MSEloss	AdamW	0.76
5		16	Huberloss	AdamW	<u>0.85</u>
6	Exp# 3	16	Huberloss	SGD	-
7		16	Huberloss	RMSprop	0.89

253 The ablation study explores the impact of various configurations on the model's performance. The base-
254 line configuration, utilizing a sample duration of 8 with the SmoothL1 loss function and AdamW optimizer,
255 achieved an R^2 score of 0.70, serving as a reference point for further variations. Table 1 summarizes the
256 experimentation.

257 **Effect of Sample duration:** Experiments were conducted to analyze the impact of varying sample
258 duration on model performance while keeping the loss function (SmoothL1), optimizer (AdamW), and
259 other hyperparameters constant. Results proved that decreasing the sample duration from 8 (baseline) to 4
260 reduced the R^2 value from 0.70 to 0.43. However, increasing the sample duration to 16 improved the R^2
261 value to 0.79. This indicates that a longer sample duration provides a better temporal context, improving
262 model performance.

263 **Impact of loss functions:** The CNN-LSTM architecture was ablated incrementally. This section ana-
264 lyzes the model performance by changing loss functions. The baseline SmoothL1 loss was replaced with
265 MSELoss and HuberLoss, while other training parameters were kept consistent, isolating the impact of the
266 loss function. The performance decreased by 3.8%, with MSELoss resulting in a R^2 score of 0.76. For Hu-
267 berLoss, the performance increased with a R^2 score of 0.85, showing a significant improvement of 7.59%.
268 This suggests that HuberLoss effectively handles deviation compared to SmoothL1 and MSELoss. While
269 MSELoss heavily penalizes large errors due to its quadratic nature, HuberLoss applies a linear penalty to
270 large residuals, thus reducing the influence of outliers more effectively. Unlike SmoothL1, which has a fixed
271 transition.

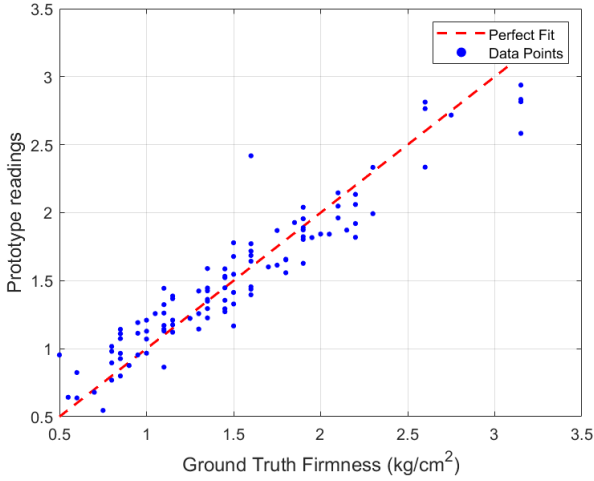


Figure 5: Correlation between the prototype readings and reference firmness values with a Coefficient of Determination (R^2) score of 0.89.

Effect of optimizers for better convergence: The impact of using different optimizers was explored while keeping the sample duration fixed at 16 and using HuberLoss. Although the model did not converge with the SGD optimizer, using RMSprop resulted in the highest R^2 score of 0.89. RMSProp adapts the learning rate for each parameter dynamically based on recent gradients. It maintains a moving average of the squared gradients, which helps stabilize updates and prevents large oscillations in the optimization process. This is particularly beneficial for datasets that contain outliers of varying scales, allowing them to converge more effectively.

Overall, the ablated model achieved a R^2 increased of 0.19 increment over the baseline. This improvement is attributed to the combination of high temporal information, Huberloss loss function for handling outliers, and RMSProp to maintain stability during training. It enhanced the model's capability to predict firmness from Palpation (video).

5. Results and Discussion

This section discusses the quantitative and qualitative results. Lastly, the comparison of our proposed model with SOTA architecture and the comparison of our proposed device all available commercials is also discussed.

5.1. Regression Analysis

In the evaluation of our video regression model, we conducted a comprehensive residual analysis to assess the discrepancies between the model predictions and the observed ground truth values. The scatter plot, Figure 6, of residuals versus ground truth demonstrates a generally random distribution of residuals across different ground truth values, suggesting that our model does not exhibit systematic bias across the range of outputs. This is further corroborated by the histogram of residuals, which shows a distribution centered around zero with most residuals tightly clustered within a narrow range, albeit with slight skewness. This distribution suggests that, while our model is generally accurate and unbiased, there remains some variability in prediction accuracy.

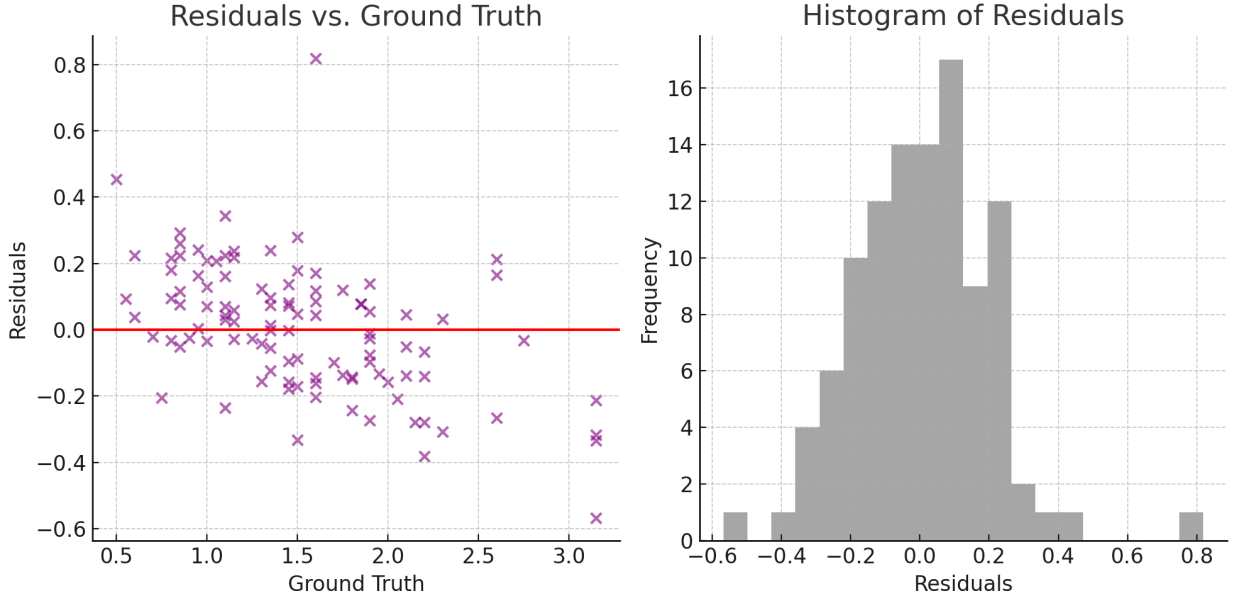


Figure 6: Residual Analysis of our model **(Left)** Scatter plot of residuals demonstrates random distribution suggesting unbiased model estimation. **(Right)** The Histogram of Residuals shows residuals centered around zero, indicating general estimation accuracy with slight variability.

296 Figure 5 illustrates the correlation between the firmness readings of the proposed model and the ground
 297 truth. The red dashed line represents the ideal 1:1 correlation, and the blue data points indicate the predictions,
 298 which closely follow the trend of the perfect fit line, demonstrating a strong positive correlation. A
 299 R^2 score of 0.89 was achieved.

300 5.2. Palpation Explainability and Interpretability Analysis

301 To assess our model's ability to capture human palpation motions from DIGIT video sequences, we uti-
 302 lized Grad-CAM (Selvaraju et al. 2017) using the TorchCAM library (Fernandez 2020). Figure 7 showcases
 303 samples with varying firmness levels and corresponding spatial attention patterns. In each frame, the left
 304 image represents the input from the DIGIT sensor, while the right picture shows the overlay of the model's
 305 attention using Grad-CAM. This visualization technique highlights image regions most influential to the
 306 model's predictions. This allowed us to confirm whether the model aligns its focus with the DIGIT sensor
 307 motion during palpation.

308 For the first sample, the ground truth firmness was 2.75, and the model predicted 2.71, resulting in a
 309 residual of 0.03. In the second sample, the residual was only 0.02. Both samples exhibit strong spatial
 310 alignment between the model's attention and the palpation regions, indicating that the model effectively
 311 captures relevant palpation deformation for accurate firmness prediction. Conversely, in the third sample,
 312 the residual was 0.29. As shown in Figure 7, the model's attention is less aligned with the palpation region in
 313 this sample, contributing to a higher residual error. Overall, the consistent attention patterns in well-aligned
 314 cases highlight the model's generalization capability and reliability in analyzing palpation dynamics, while
 315 misalignments suggest areas for further improvement in handling diverse firmness conditions.

316 Lastly, we analyse the impact of duration of palpation on prediction of firmness. Figure 8 displays
 317 the relationship between the number of frames in a video and the prediction residuals of our regression
 318 model. The red line, which represents a smoothed trend of the residuals, exhibits a slight peak around

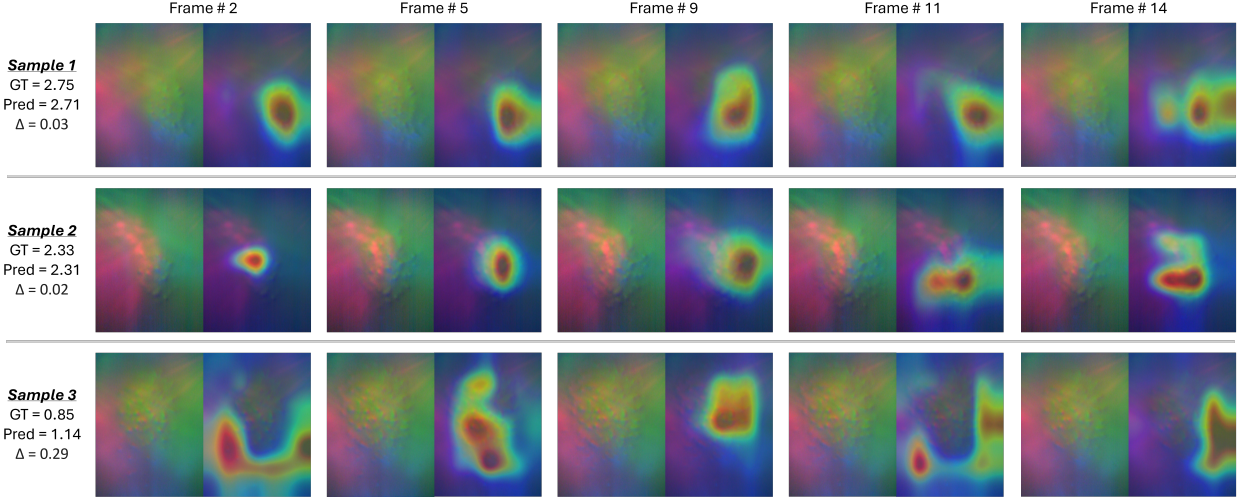


Figure 7: Grad-CAM Visualizations of our proposed model: Each row represents a unique sample with corresponding ground-truth (GT) and predicted (Pred) firmness values, along with the residuals (Δ). The left image in each frame shows the input VBTS image, while the right image displays the model’s attention overlay using Grad-CAM. The Grad-CAM visualizations highlight the spatial alignment between the model’s attention and the palpation region on VBTS images. In Samples 1 and 2, strong alignment correlates with accurate estimation and low residuals. Conversely, Sample 3 shows poor alignment, resulting in higher residual error. The frames displayed correspond to the sequence’s 2nd, 5th, 9th, 11th, and 14th positions.

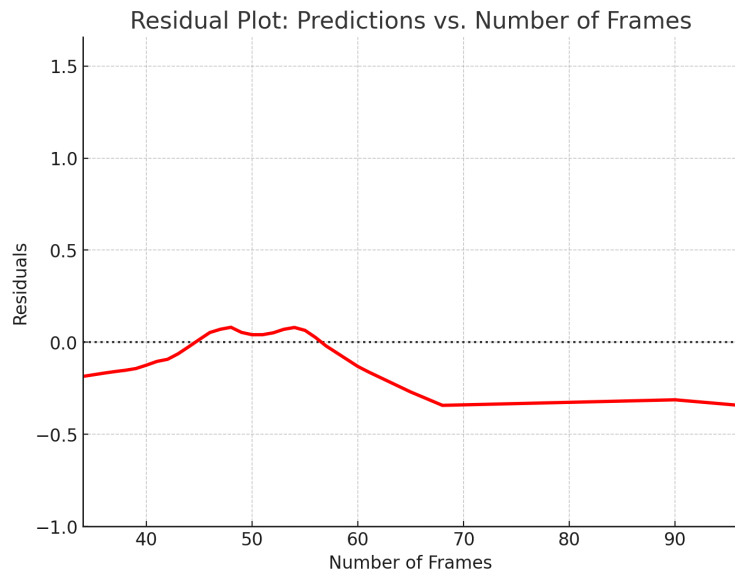


Figure 8: Residual plot of proposed model firmness estimation vs. Number of Frames - Shows minimal discrepancies at around 50 frames, stabilizing in longer videos. Indicates minimal impact of frame count on model accuracy.



Figure 9: Comparison of the proposed wearable device and traditional fruit firmness testers. The proposed device integrates human dexterity with AI-driven tactile sensing, enabling non-destructive, real-time firmness estimation. In contrast, conventional methods—including mechanical (rupture and durometer), optical, and vibrational techniques are often invasive or influenced by environmental factors, limiting their adaptability and accuracy.

319 50 frames, indicating minor discrepancies in predictions in this range. However, as the number of frames
 320 increases beyond this point, the residuals trend towards zero, suggesting that the model predictions become
 321 more accurate or consistent with the actual values. This pattern implies that the model may handle longer
 322 sequences slightly better, possibly due to more comprehensive data within these videos. Nevertheless,
 323 the overall trend is relatively flat, confirming that the number of frames does not significantly affect the
 324 prediction residuals, indicating minimal influence on model performance across different video lengths. It's
 325 important to note that while the FPS of the DIGIT sensor was set to 30, we cannot confirm if this was
 326 maintained in real time since the actual duration of palpation was not recorded. As explained in Section
 327 3.4, our dataset only contains frames of palpation, and the number of frames serves as an indicator of the
 328 duration of palpation.

329 This analysis confirms that the model focuses on relevant spatial and temporal features related to human
 330 palpation motions, supporting its ability to predict fruit firmness accurately.

Table 2: Evaluation of the proposed model versus SOTA architectures on MSE, RMSE, R^2 , and MAE metrics

Sr	Model	MAE ↓	RMSE ↓	R^2 ↑
1	TimesFormer (Bertasius, Wang, and Torresani 2021)	0.17	0.21	0.87
2	VideoMAE (Tong et al. 2022)	0.22	0.28	0.78
3	Ours <i>Baseline</i>	0.24	0.33	0.70
4	Ours <i>Improved</i>	0.15	0.20	0.89

331 5.3. Comparative Analysis

332 The performance of the proposed CNN-LSTM model was evaluated through a comparative analysis
 333 with transformer based architectures, specifically TimesFormer (Bertasius, Wang, and Torresani 2021) and
 334 VideoMAE (Tong et al. 2022), which represent the state-of-the-art in video-based tasks. To ensure a rigorous
 335 and equitable comparison, these transformer models were fine-tuned on the dataset used in this study,

Table 3: Qualitative comparison of portable commercial devices used for fruit firmness detection.

Sr	Mechanism	Name	Non-Destructive	Compact	Wearable	On-tree	AI-Based	Wireless	Accuracy	Operation	Cost	Weight (g)	Size (mm)
1	Mechanical (Rupture Force)	FT-series (QA Supplies 2024)	✗	✓	✗	✗	✗	✓	α	ω	\$\$\$\$\$	500	112*59*24
2		GY series (Handpi 2024)	✗	✓	✗	✗	✗	✓	α	ω	\$\$\$\$\$	500	140*60*30
3		FHT series (Landtek 2024)	✗	✓	✗	✗	✗	✓	α	ω	\$\$\$\$\$	200	204*62*33
4	Mechanical (Deformation)	HPEII-Fff (Bareiss 2024)	✓	✓	✗	✓	✗	✓	α	ω	\$\$\$\$\$	300	190*70*40
5		Fruit Firm Meter (Turoni 2024)	✓	✓	✗	✓	✗	✓	α	ω	\$\$\$\$	-	-
6		Firmness Tester (Aweta 2024)	✓	✓	✗	✓	✗	✓	α	ω	\$\$\$\$	210-400	65*60*27 130*72*33
7	Acoustic/ Vibrational	Aweta AFS (Aweta 2024)	✓	✗	✗	✗	✗	✗	φ	β	-	-	-
8		MR-series (MR-Series 2024)	✓	✓	✓	✓	✗	✓	γ	-	\$\$\$\$\$	76	Wearable
10	Optical	F-750 (Felix 2024)	✓	✗	✗	✓	✗	✓	φ	φ	\$\$\$\$\$	1050	180*120*45
11		NIR Case (Sacmi 2024)	✓	✗	✗	✗	✗	✗	φ	ω	-	NA	400*300*200
12		DA-meter (T. T. Store 2024)	✓	✓	✗	✓	✗	✓	φ	φ	-	320	165*80*50
13	Vision-based tactile sensing	Ours	✓	✓	✓	✓	✓	✓	φ	φ	\$\$\$\$\$	135	Wearable

Notes: In the 'Accuracy Limitations' column, symbols represent specific conditions: 'α' indicates that additional apparatus is necessary to enhance accuracy, 'γ' suggests that the accuracy of the measurement is affected by contact, and 'φ' signifies none of the aforementioned conditions apply. In the 'Operation Limitations' column, 'ω' denotes that additional assembly of components is required for handling different fruits, 'β' implies additional measurements related to the shape and weight of the fruit are necessary, and 'φ' indicates none of the mentioned limitations are applicable. In the 'Cost' column, prices are indicated as follows: \$ = under \$1,000; \$\$ = \$1,000-\$1,999; \$\$\$ = \$2,000-\$2,999; \$\$\$\$ = \$3,000-\$4,999; \$\$\$\$\$ = over \$5,000.

utilizing their pre-trained baseline weights to leverage the benefits of extensive prior training on large-scale datasets.

Our proposed model outperformed both transformers in terms of accuracy and error metrics. Specifically, our improved model achieved the lowest MAE of 0.15, RMSE of 0.20, and the highest R^2 value of 0.89. In contrast, TimesFormer achieved an MAE of 0.17 and RMSE of 0.21, with an R^2 of 0.87, while VideoMAE reported an MAE of 0.22, RMSE of 0.28, and R^2 of 0.78. These results indicate that our model provides a more precise and reliable prediction. Table 2 compares our proposed model with SOTA models.

5.4. Comparison with Commercial Devices

The proposed thumb-mounted device for the estimation of fruit firmness is compared to existing portable commercial devices in Table 3. These devices, widely used in the agricultural industry, serve as benchmarks for practical applications (see Figure 9). Key attributes considered in the comparison include non-destructiveness, compactness, wearability, on-tree measurement capability, AI integration, wireless functionality, ease of operation, and cost-effectiveness. Non-destructiveness preserves fruit quality, compactness, and wearability, enhancing usability, and on-tree measurement capability allows immediate field data collection. AI integration improves accuracy, wireless functionality simplifies data management, ease of operation ensures accessibility for diverse users, and cost-effectiveness broadens adoption.

Table 3 details the evaluation of these attributes and reveals notable limitations in existing devices. Mechanical penetrometers (e.g., FT-series, GY series, FHT series) are compact, wireless, and low-cost but destructive, non-wearable, and lack on-tree measurement capability. Mechanical durometers (e.g., HPEII-Fff, Fruit Firm Meter, Firmness Tester) are compact, wireless, and support on-tree measurements but are not wearable and require additional apparatus for accuracy. Acoustic/vibrational devices vary: the Aweta AFS



Figure 10: On-tree demonstration of the wearable device for real-time kiwifruit firmness assessment. This figure shows the device in a field setting, estimating firmness directly on the tree using palpation-based sensing. The battery-powered, wrist-worn design supports portable, non-destructive use. The setup demonstrates on-tree feasibility.

357 is non-destructive but bulky, non-wearable, and requires additional shape and weight measurements, while
 358 the MR-series is compact, wearable, and wireless but has accuracy limitations and is high-cost. Optical
 359 devices (e.g., F-750, NIR Case, DA-meter) are non-destructive, with the DA-meter being compact and
 360 wireless, while others are larger and may require assembly for different fruits.

361 In contrast, our device stands out by incorporating all key attributes—it is non-destructive, compact,
 362 wearable, supports on-tree measurements, and is wireless. It has no noted accuracy or operational limita-
 363 tions and employs a palpation-based method, making it unique among the compared devices. In addition,
 364 the cost is low.

365 Lastly, the global fruit firmness tester market was valued at 72.3 million USD in 2023 and is projected
 366 to reach 110.2 million USD by 2032 (More 2024). This growth underscores the increasing demand for
 367 non-destructive firmness testers, highlighting the market potential and relevance of the proposed device as
 368 an innovative and practical solution for the agriculture industry.

369 6. Real World Demonstration

370 To evaluate the device’s practical utility in agriculture, we conducted on-tree firmness assessments of
 371 kiwifruit without detaching or damaging them—highlighting the non-destructive nature of our approach and
 372 its relevance for precision harvest decisions. As shown in Figure 10, three kiwifruits were suspended from
 373 a tree for testing. The operator donned the wrist and thumb modules, completing setup in 30 ± 11 seconds.
 374 Firmness estimation involved gently grasping a fruit, initiating the process via a button press, and receiving
 375 real-time prompts and haptic feedback. The SBC verified sensor status, captured tactile data, ran the deep
 376 learning model, and displayed the predicted firmness within 18.25 ± 0.16 seconds. Including a 5-second
 377 display period, the full interaction loop lasted 23.98 ± 0.31 seconds. Model inference time was $3.82 \pm$
 378 0.27 seconds, with a computational complexity of 5.01 GFLOPs for 16 frames (0.3128 GFLOPs/frame),
 379 measured using the FVCORE library (Research 2019).

380 The operator applied minimal force (2–10 N) with brief short palpation durations to minimize bruising.
 381 No wrist or thumb strain was reported, and the fruits showed no visible damage, validating the device’s

382 comfort and safety for on-tree use.

383 **7. Limitations and Future Work**

384 While the results are promising, this study is currently limited to only "Hayward" kiwifruit. Future work
385 will aim to broaden the dataset by including a wider variety of fruits and vegetables in terms of size, shape,
386 and weight, such as cucumbers, tomatoes, blueberries, and strawberries, and will involve multiple users
387 to enhance device generalizability. Although the device is designed and demonstrated for non-destructive
388 on-tree firmness estimation (see Section 6), the dataset collected and the proposed model were validated on
389 harvested samples in the current study. Future work will focus on collecting a dataset of on-tree samples to
390 assess the system's effectiveness in detecting subtle firmness changes during on-tree ripening.

391 At this stage, firmness estimation is based solely on palpation data. Future iterations will explore multi-
392 modal sensing by incorporating additional cues, such as applied force or smell, to improve ripeness prediction.
393 Further enhancements in portability and efficiency are also planned through the integration of custom
394 tactile sensors and dedicated PCB miniaturization.

395 **8. Conclusion**

396 Ripeness is a key determinant of fruit quality, influencing flavor, marketability, and waste reduction.
397 However, assessing ripeness in fruits without clear visual cues is challenging, often necessitating destructive
398 firmness measurements. The standard method, a penetrometer, involves plucking sample fruits, transporting
399 them to a lab, cutting them open, and probing them—an inefficient, time-consuming process. If the sampled
400 fruits are not representative, the results may mislead harvesting decisions and contribute to unnecessary
401 waste. Humans naturally assess firmness through palpation, a non-destructive yet inconsistent approach
402 that often requires multiple attempts, increasing the risk of bruising and subjective variability.

403 This work introduces a novel wearable system that merges human tactile interaction with vision-based
404 tactile sensing and embedded deep learning. Operating on an edge computing platform, it bypasses cloud
405 dependencies, ensuring reliable use in low-connectivity environments. By embedding a DIGIT sensor at the
406 thumb tip, the device harnesses natural human dexterity, while the proposed model processes spatiotemporal
407 features of palpation to provide rapid, accurate firmness predictions. The device comprises two modules:
408 the thumb module, which houses a DIGIT sensor to capture real-time tactile images, and the wrist module,
409 which contains the controller, display, and user interface. The operator holds the kiwifruit with four fingers
410 and presses a button to initiate palpation. The embedded model then processes vision-based tactile sensing
411 (VBTS) data to predict firmness, ensuring non-destructive evaluation in a real-world agricultural setting.

412 To validate the system, a Hayward kiwifruit dataset containing 530 unique palpation-firmness pairs was
413 collected. The proposed model achieved an R^2 score of 0.89, demonstrating high accuracy. A real-world
414 demonstration confirmed the feasibility of on-tree firmness estimation. No bruising was observed, and users
415 reported the device as comfortable to wear.

416 The proposed device outperforms existing commercial fruit firmness testers by combining non-destructive,
417 compact, wearable, and wireless features with AI integration. These findings pave the way for more effi-
418 cient, consistent, and user-friendly quality assessments in the agricultural sector, addressing key limitations
419 of current fruit firmness evaluation methods. This matters at scale: WWF estimates that about 15% of food
420 is lost before it leaves the farm, largely due to poor harvest timing and limited testing tools(World Wide
421 Fund for Nature 2021). By providing quick, accurate firmness readings in the orchard, the device can curb
422 premature picking, reduce bruising, and cut pre-harvest waste, supporting more sustainable production.

423 Furthermore, cost remains the chief barrier to adoption, so recent reviews advocate interim, low-cost
424 technologies to keep expenses manageable (Oliveira, Moreira, and Silva 2021; Duckett et al. 2018). In line
425 with this need, the fruit firmness tester market was valued at USD 72.3 million in 2023 and is projected to
426 reach USD 110.2 million by 2032 (More 2024), indicating growing demand for affordable, non-destructive
427 solutions and underscoring the market potential of our device.

428 Acknowledgement

429 This publication is based upon work supported by the Khalifa University of Science and Technology under
430 Award No. RC1-2018-KUCARS.

431 Declaration of competing interest

432 The authors declare that they have no known competing financial interests or personal relationships that
433 could have appeared to influence the work reported in this paper.

434 References

- 435 Abbott, JA et al. (1995). "Nondestructive sonic firmness measurement of apples". In: *Transactions of the ASAE* 38.5. Publisher:
436 American Society of Agricultural and Biological Engineers, pp. 1461–1466.
437 Abbott, Judith A (1999). "Quality measurement of fruits and vegetables". In: *Postharvest biology and technology* 15.3. Publisher:
438 Elsevier, pp. 207–225.
439 Ahmadi, Ebrahim (2018). "Bruise susceptibilities of kiwifruit as affected by impact and fruit properties." In: *Research in Agricultural
440 Engineering*. doi: 10.17221/57/2011-RAE.
441 Anjali et al. (2024). "State-of-the-art non-destructive approaches for maturity index determination in fruits and vegetables: Principles,
442 applications, and future directions". In: *Food Production, Processing and Nutrition* 6.1. Publisher: Springer, p. 56.
443 Aweta (2024). *Aweta - sorting and packing solutions for fruit and vegetables*. URL: <https://www.aweta.com/en/> (visited on
444 05/22/2024).
445 Bareiss (2024). *Fruit Firmness Tester - HPE III Fff - Bareiss North America*. URL: <https://www.bareiss-testing.com/product/fruit-firmness-tester-hpe-iii-fff/> (visited on 05/22/2024).
446 Barrett, Diane M., Elisabeth Garcia, and Jo Ellen Wayne and (1998). "Textural Modification of Processing Tomatoes". In: *Critical
447 Reviews in Food Science and Nutrition* 38.3. Publisher: Taylor & Francis .eprint: <https://doi.org/10.1080/10408699891274192>,
448 pp. 173–258. doi: 10.1080/10408699891274192. URL: <https://doi.org/10.1080/10408699891274192>.
449 Bertasius, Gedas, Heng Wang, and Lorenzo Torresani (2021). "Is space-time attention all you need for video understanding?" In:
450 *ICML*. Vol. 2. Issue: 3, p. 4.
451 Cirilli, Marco et al. (2016). "On-field monitoring of fruit ripening evolution and quality parameters in olive mutants using a portable
452 NIR-AOTF device". In: *Food chemistry* 199. Publisher: Elsevier, pp. 96–104.
453 Condon, Melia et al. (2014). "Differential sensitivity to surface compliance by tactile afferents in the human finger pad". In: *Journal
454 of Neurophysiology* 111.6. Publisher: American Physiological Society Bethesda, MD, pp. 1308–1317.
455 Duckett, Tom et al. (2018). "Agricultural robotics: the future of robotic agriculture". In: *arXiv preprint arXiv:1806.06762*.
456 Felix (2024). *F-750 Produce Quality Meter - Felix Instruments*. URL: <https://felixinstruments.com/food-science-instruments/nir-spectroscopy/f-750-produce-quality-meter/> (visited on 05/22/2024).
457 Fernandez, François-Guillaume (Mar. 2020). *TorchCAM: class activation explorer*. URL: <https://github.com/frgfm/torchcam>.
458 Garcia, Coralía V. et al. (2012). "Kiwifruit flavour: A review". In: *Trends in Food Science & Technology* 24.2, pp. 82–91. ISSN:
459 0924-2244. doi: <https://doi.org/10.1016/j.tifs.2011.08.012>. URL: <https://www.sciencedirect.com/science/article/pii/S0924224411002445>.
460 Handpi (2024). *Handpi - The Force Gauge and Torque Gauge Specialists - Force & torque testing solutions - worldwide*. URL:
461 <http://www.handpi.com/en/Productshow.asp?ArticleID=303> (visited on 05/22/2024).
462 Harker, F. R. and Ian C. Hallett (1994). "Physiological and Mechanical Properties of Kiwifruit Tissue Associated with Texture
463 Change during Cool Storage". In: *Journal of the American Society for Horticultural Science*. doi: 10.21273/JASHS.119.5.
464 987.
465

- 469 Harker, FR, JH Maindonald, and PJ Jackson (1996). "Penetrometer measurement of apple and kiwifruit firmness: operator and
 470 instrument differences". In: *Journal of the American Society for Horticultural Science* 121.5. Publisher: American Society for
 471 Horticultural Science, pp. 927–936.
- 472 Howard, Andrew G. et al. (2017). *MobileNets: Efficient Convolutional Neural Networks for Mobile Vision Applications*. eprint:
 473 1704.04861. URL: <https://arxiv.org/abs/1704.04861>.
- 474 Huang, Yuping, Renfu Lu, and Kunjie Chen (2018). "Prediction of firmness parameters of tomatoes by portable visible and near-
 475 infrared spectroscopy". In: *Journal of food engineering* 222. Publisher: Elsevier, pp. 185–198.
- 476 Huber, Peter J (1992). "Robust estimation of a location parameter". In: *Breakthroughs in statistics: Methodology and distribution*.
 Springer, pp. 492–518.
- 477 Jantra, Chaiya et al. (2018). "Development of a handheld precision penetrometer system for fruit firmness measurement". In:
 478 *Postharvest Biology and Technology* 144. Publisher: Elsevier, pp. 1–8.
- 480 Khalifa, Smail, Mohammad Hassan Komarizadeh, and Behrouz Tousi (2011). *Review article Usage of fruit response to both force
 481 and forced vibration applied to assess fruit firmness- a review*.
- 482 Khalifa, Smail, Mohammad Hasan Komarizadeh, and Behrouz Tousi (2011). "Usage of fruit response to both force and forced
 483 vibration applied to assess fruit firmness-a review". In: *Australian Journal of Crop Science* 5.5. Publisher: Southern Cross
 484 Publishers Lismore, NSW, pp. 516–522.
- 485 Khan, Asim et al. (2023). "Tomato maturity recognition with convolutional transformers". In: *Scientific reports* 13.1. Publisher:
 486 Nature Publishing Group UK London, p. 22885.
- 487 Lambeta, Mike et al. (2020). "DIGIT: A Novel Design for a Low-Cost Compact High-Resolution Tactile Sensor With Application
 488 to In-Hand Manipulation". In: doi: 10.1109/LRA.2020.2977257.
- 489 Landtek (2024). *Fruit Hardness Tester FHT-05, FHT-15, FHT-1122 Catalog*. URL: https://www.landtek.cn/FruitHardnessTester_FHT-05_FHT-15_FHT-1122_Catalog.pdf (visited on 05/22/2024).
- 491 Li, Huajia et al. (2016). "Kiwifruit firmness: Measurement by penetrometer and non-destructive devices". In: *Postharvest Biology
 492 and Technology* 120. Publisher: Elsevier, pp. 127–137.
- 493 Li, Song et al. (2023). "Assessing fruit hardness in robot hands using electric gripper actuators with tactile sensors". In: doi:
 494 10.1016/j.sna.2023.114843.
- 495 Lin, Chien-Der et al. (June 7, 2018). *Agricultural product detection device, agricultural product management system and method
 496 thereof*.
- 497 Lin, Jiahao et al. (2023). "Non-destructive fruit firmness evaluation using a soft gripper and vision-based tactile sensing". In:
 498 *Computers and Electronics in Agriculture*. doi: 10.1016/j.compag.2023.108256.
- 499 Ma, Chan, Yibin Ying, and Lijuan Xie (2024). "Visuo-tactile sensor development and its application for non-destructive measure-
 500 ment of peach firmness". In: *Computers and Electronics in Agriculture*. doi: 10.1016/j.compag.2024.108709.
- 501 Magness, John Robert and George F Taylor (1925). "An improved type of pressure tester for the determination of fruit maturity".
 In.
- 503 Mazhar, M. et al. (2016). "Comparison of firmness meters for measuring 'Hass' avocado fruit firmness". In: doi: 10.17660/
 504 ACTAHORTIC.2016.1119.22.
- 505 Mohsan, Mashhood M. et al. (2025). "SwishFormer for robust firmness and ripeness recognition of fruits using visual tactile im-
 506 agery". In: *Postharvest Biology and Technology* 225, p. 113487. ISSN: 0925-5214. doi: <https://doi.org/10.1016/j.postharvbio.2025.113487>. URL: <https://www.sciencedirect.com/science/article/pii/S0925521425000997>.
- 508 More, Anuradha B. (2024). *Fruit Firmness Tester Market: Global Industry Analysis, Size, Share, Growth, Trends, and Forecast*.
 URL: <https://dataintelo.com/report/global-fruit-firmness-tester-market>.
- 510 Nazir, Mian Faisal et al. (2024). "Kiwifruit in the Omics Age: Advances in Genomics, Breeding, and Beyond". In: *Plants*. doi:
 511 10.3390/plants13152156.
- 512 Oliveira, Luiz FP, António P Moreira, and Manuel F Silva (2021). "Advances in agriculture robotics: A state-of-the-art review and
 513 challenges ahead". In: *Robotics* 10.2. Publisher: MDPI, p. 52.
- 514 Peleg, Kalman (Nov. 25, 1997). *Method and equipment for measuring firmness of fruits and vegetables*.
- 515 Pinto, Ciro Martins et al. (May 2014). *BR102014013727A2 - Wearable glove for analysis and classification of agricultural products
 516 - Google Patents*. URL: <https://patents.google.com/patent/BR102014013727A2/en?oq=BR102014013727A2>.
- 517 QA Supplies (2024). *FT 011 Penetrometer*. URL: <https://qasupplies.com/ft-011-penetrometer/> (visited on 05/22/2024).
- 518 Research, Facebook AI (2019). *fvcore: A collection of common code for deep learning research*. URL: <https://github.com/facebookresearch/fvcore>.
- 520 Rivera, Sebastian et al. (2023). "Instrumental mechanical parameters related to hand-feel touch firmness of blueberries". In:
 521 *Postharvest Biology and Technology* 205, p. 112530. ISSN: 0925-5214. doi: <https://doi.org/10.1016/j.postharvbio.2023.112530>. URL: <https://www.sciencedirect.com/science/article/pii/S0925521423002910>.
- 523 Sacmi (2024). *NIR inspection systems by Sacmi*. URL: <https://www.sacmi.com/en-US/corporate/news/5819/NIR-inspection-systems-by-Sacmi> (visited on 05/22/2024).

- 525 Selvaraju, Ramprasaath R et al. (2017). “Grad-cam: Visual explanations from deep networks via gradient-based localization”. In: *Proceedings of the IEEE international conference on computer vision*, pp. 618–626.
- 526 MR-Series (2024). *MRI series*. URL: <https://www.ava.co.jp/yubi> (visited on 04/24/2024).
- 527 Supplies, Q. A. (n.d.). *FT 327 Penetrometer*. Accessed: 2025-04-09. URL: <https://qasupplies.com/ft327-penetrometer/>.
- 528 T. T. Store (2024). *DA Meter*. URL: <https://www.trturoni.com/en/fruit-veg-ripeness-quality-control/da-meter/da-meter.5.html> (visited on 05/22/2024).
- 529 Tong, Zhan et al. (2022). “Videomae: Masked autoencoders are data-efficient learners for self-supervised video pre-training”. In: *Advances in neural information processing systems* 35, pp. 10078–10093.
- 530 Turoni (2024). *TR Turoni 53225 Fruit Firm Hardness Tester for Kiwi, Blueberries, Cherries and more*. URL: <https://tinyurl.com/tn96dym4> (visited on 05/22/2024).
- 531 Valiente, L. D., K. M. R. Parco, and G. C. P. Sangalang (Oct. 2021). “Non-destructive Image Processing Analysis for Defect Identification and Maturity Detection on Avocado Fruit”. In: *2021 5th International Conference on Communication and Information Systems (ICCIS)*, pp. 175–179. doi: 10.1109/ICCIS53528.2021.9645970.
- 532 Voss, Monica et al. (2024). “Unlocking the Potential of Agrifood Waste for Sustainable Innovation in Agriculture”. In: *Recycling*. doi: 10.3390/recycling9020025.
- 533 World Wide Fund for Nature (July 2021). *Over 15% of food is lost before leaving the farm - WWF report*. URL: <https://www.wwf.eu/?4049841/fifteen-per-cent-of-food-is-lost-before-leaving-the-farm-WWF-report>.
- 534 Xu, Chang et al. (2020). “Tactile Exploration Strategies With Natural Compliant Objects Elicit Virtual Stiffness Cues”. In: *IEEE Transactions on Haptics* 13.1, pp. 4–10. doi: 10.1109/TOH.2019.2959767.
- 535 Yuan, Wenzhen, Mandayam A. Srinivasan, and Edward H. Adelson (2016). “Estimating object hardness with a GelSight touch sensor”. In: *2016 IEEE/RSJ International Conference on Intelligent Robots and Systems (IROS)*, pp. 208–215. doi: 10.1109/IROS.2016.7759057.
- 536 Yuan, Wenzhen, Chenzhuo Zhu, et al. (2017). “Shape-independent hardness estimation using deep learning and a GelSight tactile sensor”. In: *2017 IEEE International Conference on Robotics and Automation (ICRA)*, pp. 951–958. doi: 10.1109/ICRA.2017.7989116.
- 537 Zhao, Zikai et al. (Apr. 2024). “Exploring Embodied Intelligence in Soft Robotics: A Review”. In: *Biomimetics* 9. doi: 10.3390/biomimetics9040248. URL: <https://www.mdpi.com/2313-7673/9/4/248/pdf?version=1713539955>.